

DTIC COPY

2



AD-A222 803

WRDC-TR-90-4013

FRACTURE TOUGHNESS AND FAILURE MECHANISMS IN
COMMERCIAL 2091 Al-Li SHEET AT CRYOGENIC TEMPERATURES

Kumar V. Jata
John J. Ruschau

University of Dayton
Research Institute
300 College Park Avenue
Dayton, Ohio 45469

DTIC
ELECTE
JUN 18 1990
S D
D

MARCH 1990

Interim Report for Period July 1988 - December 1989

Approved for public release; distribution unlimited.

MATERIALS LABORATORY
WRIGHT RESEARCH AND DEVELOPMENT CENTER
AIR FORCE SYSTEMS COMMAND
WRIGHT-PATTERSON AIR FORCE BASE, OH 45433-6533

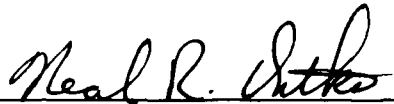
90 60 10 034

NOTICE

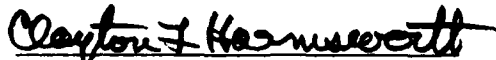
When Government drawings, specifications, or other data are used for any purpose other than in connection with a definitely Government-related procurement, the United States Government incurs no responsibility or any obligation whatsoever. The fact that the government may have formulated or in any way supplied the said drawings, specifications, or other data, is not to be regarded by implication, or otherwise in any manner construed, as licensing the holder, or any other person or corporation; or as conveying any rights or permission to manufacture, use, or sell any patented invention that may in any way be related thereto.

This report is releasable to the National Technical Information Service (NTIS). At NTIS, it will be available to the general public, including foreign nations.

This technical report has been reviewed and is approved for publication.

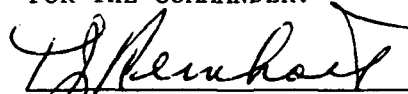


NEAL R. ONTKO
Program Manager
Materials Engineering Branch



CLAYTON L. HARMSWORTH
Technical Manager
Engineering and Design Data
Materials Engineering Branch

FOR THE COMMANDER:



T. J. REINHART, Chief
Materials Engineering Branch

If your address has changed, if you wish to be removed from our mailing list, or if the addressee is no longer employed by your organization, please notify WRDC/MLSE, WPAFB, OH 45433-6533 to help us maintain a current mailing list.

Copies of this report should not be returned unless return is required by security considerations, contractual obligations, or notice on a specific document.

UNCLASSIFIED

SECURITY CLASSIFICATION OF THIS PAGE

Form Approved
OMB No. 0704-0188

REPORT DOCUMENTATION PAGE

1a. REPORT SECURITY CLASSIFICATION Unclassified			1b. RESTRICTIVE MARKINGS			
2a. SECURITY CLASSIFICATION AUTHORITY			3. DISTRIBUTION / AVAILABILITY OF REPORT Approved for public release; distribution unlimited.			
2b. DECLASSIFICATION / DOWNGRADING SCHEDULE			4. PERFORMING ORGANIZATION REPORT NUMBER(S) UDR-TR-90-04			
4. PERFORMING ORGANIZATION REPORT NUMBER(S) UDR-TR-90-04			5. MONITORING ORGANIZATION REPORT NUMBER(S) WRDC-TR-90-4013			
6a. NAME OF PERFORMING ORGANIZATION University of Dayton Research Institute		6b. OFFICE SYMBOL (if applicable)	7a. NAME OF MONITORING ORGANIZATION Wright Research and Development Center Materials Laboratory (WRDC/MLSE)			
6c. ADDRESS (City, State, and ZIP Code) 300 College Park Avenue Dayton, OH 45469			7b. ADDRESS (City, State, and ZIP Code) Wright-Patterson AFB, OH 45433-6533			
8a. NAME OF FUNDING / SPONSORING ORGANIZATION Wright Research and Develop. Ctr., Materials Lab (WRDC/MLSE)		8b. OFFICE SYMBOL (if applicable) WRDC/MLSE	9. PROCUREMENT INSTRUMENT IDENTIFICATION NUMBER F33615-88-C-5437			
8c. ADDRESS (City, State, and ZIP Code) Wright-Patterson AFB, OH 45433-6533			10. SOURCE OF FUNDING NUMBERS			
		PROGRAM ELEMENT NO. 62102F	PROJECT NO. 2418	TASK NO. 07	WORK UNIT ACCESSION NO. 03	
11. TITLE (Include Security Classification) Fracture Toughness and Failure Mechanisms in Commercial 2091 Al-Li Sheet at Cryogenic Temperatures						
12. PERSONAL AUTHOR(S) Kumar V. Jata and John J. Ruschau						
13a. TYPE OF REPORT Interim		13b. TIME COVERED FROM 7/88 TO 12/89		14. DATE OF REPORT (Year, Month, Day) March 9, 1990		15. PAGE COUNT 46
16. SUPPLEMENTARY NOTATION						
17. COSATI CODES			18. SUBJECT TERMS (Continue on reverse if necessary and identify by block number)			
FIELD	GROUP	SUB-GROUP	Aluminum-Lithium, Fracture Toughness, Fracture			
11	04		2091-T3, Cryogenic Temperatures, mechanisms			
			Sheet, Tensile, Mechanical Properties, Alloys			
19. ABSTRACT (Continue on reverse if necessary and identify by block number) Aluminum-Lithium millimeters Strength-toughness relationships in 2091 Al-Li alloy in the T3 temper were examined at ambient, liquid nitrogen and liquid helium temperatures as a function of sheet orientation and product form (sheet thickness). Commercially available 1.6 mm (0.063 inch) and 3.6 mm (0.144 inch) thick sheets in the T3 temper were examined, with both alloy sheets exhibiting increasing yield strength but decreasing tensile elongation and toughness at cryogenic temperatures in all orientations. This behavior is in contrast with the observation of enhanced strength and toughness in longitudinal and transverse orientations (L-T and T-L) and certain heat treatment tempers of 2090 and 8090 Al-Li alloys at cryogenic temperatures. It is also noted that in the present 2091 sheets where the triaxial state of stress is expected to be low, through thickness delaminations are prevalent at cryogenic temperatures due to weak short transverse properties. However, these delaminations and enhanced strain hardening exponents do not provide toughness enhancement at liquid nitrogen and liquid helium temperatures. (Continued on reverse side)						
20. DISTRIBUTION / AVAILABILITY OF ABSTRACT <input checked="" type="checkbox"/> UNCLASSIFIED/UNLIMITED <input type="checkbox"/> SAME AS RPT. <input type="checkbox"/> DTIC USERS			21. ABSTRACT SECURITY CLASSIFICATION Unclassified			
22a. NAME OF RESPONSIBLE INDIVIDUAL Clayton L. Harmsworth			22b. TELEPHONE (Include Area Code) 513-255-5063		22c. OFFICE SYMBOL WRDC/MLSE	

DD Form 1473, JUN 86

Previous editions are obsolete.

SECURITY CLASSIFICATION OF THIS PAGE

UNCLASSIFIED

UNCLASSIFIED

19. ABSTRACT (Concluded)

The decrease in toughness observed in the present 2091 sheets is due to a change from ductile fracture mode at ambient temperature to a brittle fracture mode at cryogenic temperatures.

PREFACE

This technical report represents work conducted by the University of Dayton Research Institute under contract to the Wright Research and Development Center, Materials Laboratory, Systems Support Division, Contract F33615-88-C-5437, "Quick Reaction Evaluation of Materials." Mr. Neal Ontko was the contract monitor.

This effort was conducted during the period of July 1988 to December 1989. The authors, Dr. Kumar V. Jata and Mr. John J. Ruschau, would like to extend special recognition to Messrs. Kevin Osborne, James Peters, and John Eblin of the University of Dayton who were responsible for all testing and data reduction.

This report was submitted by the authors in January 1990.



Accession For	
NTIS CRA&I	<input checked="" type="checkbox"/>
DTIC TAB	<input type="checkbox"/>
Unannounced	<input type="checkbox"/>
Justification	
By	
Distribution/	
Availability Codes	
Dist	Avail and/or Special
A-1	

TABLE OF CONTENTS

<u>SECTION</u>		<u>PAGE</u>
1	INTRODUCTION.....	1
2	BACKGROUND.....	2
3	EXPERIMENTAL PROCEDURES.....	5
4	RESULTS AND DISCUSSION.....	7
5	REMARKS ON PRESENT FINDINGS.....	34
6	CONCLUSIONS.....	36
	REFERENCES.....	37

LIST OF FIGURES

<u>FIGURE</u>		<u>PAGE</u>
1	Optical Microstructure Showing the Grain Structure in the 3.6 mm (a) and 1.6 mm (b), Thick 2091 Sheet Alloy.....	9
2	Variation of Yield (YS) and Ultimate Tensile Strengths (UTS) and Percent Elongation as a Function of Specimen Orientation at 294K and 77K.....	11
3	Effect of Temperature on the Tensile Properties in the Longitudinal and Long-Transverse Orientation for the 3.6 mm and Longitudinal Orientation for 1.6 mm.....	13
4	TEM Micrographs Showing the Dislocation Structures at 294K and 77K.....	14
5	Low Magnification Fractographs in Longitudinal Tensile Samples at (a) Room Temperature, (b) Liquid Nitrogen, (c) Liquid Helium Temperatures. Note Delamination in (b) and (c). Figure 5(d) Shows the Ductile Failure at Room Temperature and 5(e) and 5(f) Show the Brittle Failure at Cryogenic Temperatures.....	15
6	Effect of Orientation on the R-Curves at 294K and 77K for the 3.6 mm Sheet.....	16
7	Effect of Temperature (294 vs. 77K) on the R-Curves for (a) 0°, (b) 30°, (c) 45°, (d) 60°, and (e) 90° Orientations, for the 3.6 mm Sheet.....	18
8	Effect of Orientation on the R-Curves at 294 and 77K for the 1.6 mm Sheet.....	20
9	Effect of Temperature (294 vs. 77K) on the R-Curves (a) 0°, (b) 45°, (c) 60°, and (d) 90° Orientations for the 1.6 mm Sheet.....	21
10	Comparison of R-Curve Behavior of the 3.6 mm Sheet Reduced to 1.6 mm and Tested in Center Cracked Specimen Configuration, to the R-Curve Behavior of 1.6 mm Sheet. Note that although the shape is similar Kr-maximum for the 1.6 mm sheet is higher (see text).....	25

LIST OF FIGURES (Concluded)

<u>FIGURE</u>		<u>PAGE</u>
11	Load Versus Crack Opening Displacement Curves for Two Center Cracked Panels (45° Orientation) with Similar Fatigue Precrack Lengths Showing the Inability to Sustain Stable Crack Extension at Liquid Nitrogen Temperature. Notice in the Fractographs the Ductile Failure Mode at 294K and Brittle Failure Mode at 77K.....	27
12	SEM Fractographs Showing (a) Failure by Ductile Microvoid Coalescence at 294K and (b) Brittle Intergranular and Slip Band Cracking at 77K, for the 0° Oriented R-Curve Specimen.....	28
13	SEM Fractographs Showing (a) the Ductile Microvoid Coalescence with Delaminations Associated with Grain Boundaries at 294K and (b) Larger Number of Delaminations with Brittle Intergranular and Slip Band Cracking at 77K.....	29
14	Mechanism of Failure in the 45° Oriented R-Curve Specimen at 294K (a) and 77K (b) is Similar to That of the 30° Oriented Specimen.....	30
15	SEM Fractographs Showing (a) Larger Number of Delaminations Occurring at 294K in the 60° Oriented R-Curve Specimen as Compared (b) Brittle Failure and Delaminations at 77K.....	31
16	SEM Fractographs Showing that the Failure at (a) 294K in 90° Oriented R-Curve Specimen is Largely by Delaminations and Some Microvoid Coalescence; and at 77K Brittle Failure with Delaminations (b).....	32
17	Values of Kr-25% and Kr-maximum at 294K and 77K as a Function of Orientation of the 3.6 mm R-Curve Specimens, (a) and (b); and Kr-maximum Values for the 1.6 mm Sheet (c).....	33
18	Macrophotographs Showing Delaminations in Both (a) 1.6 mm and (b) 3.6 mm Sheets.....	35

LIST OF TABLES

<u>TABLE</u>		<u>PAGE</u>
1	Nominal Chemical Composition of 2091 Sheets in Weight Percent.....	8
2	Tensile Properties of the 3.6 mm and 1.6 mm 2091 Sheets at 294K, 77K and 4K.....	10
3	Kr-25% and Kr-max Values at 294K and 77K at Various Orientations for the 3.6 mm Thick 2091-T3 Alloy, C(T) Specimens.....	23
4	Kr-max Values at 294K and 77K at Various Orientations for the 1.6 mm Thick 2091-T3 Alloy, M(T) Specimens....	24

SECTION 1
INTRODUCTION

It is widely recognized that for the past 25 years, several aluminum alloys have reliably served the purpose of storing liquid cryogenic fuels such as hydrogen, oxygen and natural gas. Even today, 2219 aluminum alloy in the T87 temper is used by NASA for the main rocket fuel tank in the Space Shuttle. The driving force behind this usage has been the excellent specific mechanical properties (i.e. properties such as modulus, yield strength, UTS, etc. normalized by density), ease of weldability and liquid oxygen compatibility. Although the latter two characteristics have not yet been convincingly proven for the Al-Li alloys in commercial production, mechanical properties at cryogenic properties are comparable to the 2219 alloy. Thus Al-Li alloys originally developed for replacement of more heavier 2XXX and 7XXX aluminum alloys for airframe applications now appear to also have a potential application in the handling of cryogenic fuels and cryogenic applications in general.

In the past few years mechanical behavior and fracture mechanisms at cryogenic temperatures have been reported, for the 2090, 2091, and 8090 Al-Li alloys in plate product form (1-6). Although improved cryogenic behavior has generally been observed, there is no consensus on the cryogenic fracture mechanisms for Al-Li alloys. Secondly, cryogenic mechanical behaviour for sheet product of Al-Li alloys is lacking. This investigation was therefore aimed (1) at filling the gap in knowledge on the mechanical behavior of Al-Li sheet product forms at cryogenic temperatures and (2) understanding the fracture mechanisms associated with quasi-static loading of fracture toughness specimens.

SECTION 2 BACKGROUND

Al-Li alloys (1-6) have often been observed to exhibit much higher strength and fracture toughness at cryogenic temperatures as compared to that at ambient temperature. The superior toughness and ductility, which most often have been noted in L-T and T-L orientations, are in the range of 5 to 90 percent. The improvement in the strength, on the other hand, which has been noted in all Al-Li alloys in all tempers and orientations is of the order of 25 percent. Al-Li alloys in short-transverse orientation offer no improvement in ductility and toughness at cryogenic temperatures, but the decrease in these properties from ambient temperature values is relatively small. Combined with the fact that Al-Li alloys can provide substantial reductions in structural weight, this interesting cryogenic behavior has generated tremendous drive for use in liquid fuel, i.e. liquid hydrogen and liquid oxygen storage applications. Prior to such use, a critical issue yet remaining is the understanding of the fracture mechanisms that govern fracture toughness of Al-Li alloys at cryogenic temperatures. Since liquid helium and liquid nitrogen temperatures are approximately 20 degrees lower than liquid hydrogen and liquid oxygen, respectively, laboratory cryogenic data are extremely useful for screening purposes before additional expensive tests such as liquid oxygen compatibility (LOX) tests are performed.

Mechanisms of fracture of Al-Li alloys at cryogenic temperatures have been investigated by only a few workers in the past five years. One common observation that has been reported by all is an increase in through thickness delaminations when Al-Li alloys are tested in L-T and T-L orientations at cryogenic temperatures. These delaminations microstructurally coincide with certain high angle grain boundaries suggesting their inherent weakness under conditions of through-thickness stresses. The occurrence of delaminations has been proposed as the major mechanism for improvement in cryogenic fracture toughness. These

delaminations obviously create free surfaces and result in lowering the through-thickness constraint which changes the plane strain state of stress to plane stress. Thus once delaminations occur, a higher crack driving force is needed for sustained crack extension, resulting in a higher fracture toughness. Since higher fracture toughness is achieved via these through-thickness delaminations, this mechanism has been termed "delamination toughening" or "thin sheet toughening" (2,4,6,7).

Historically, fracture mechanisms have also been related to material deformation and material microstructure. Dislocation mechanisms explaining toughening and ductility enhancement at cryogenic temperatures have been proposed, and the mechanism has been identified as homogeneous deformation (slip) mode. Since Al-Li alloys deform by localized or heterogeneous slip mode at room temperature, the mechanism (3) is consistent with the general observation of increased strain hardening and fracture strain at cryogenic temperatures. Wider dislocation slip bands with narrower spacing at 77 K which are indicative of a homogeneous deformation mode (as compared to narrower and widely spaced slip bands at room temperature) along with higher strain hardening exponents and percent elongation in tensile specimens have been observed (6). Welpmann et al. (8) made similar observations in 8090 Al-Li alloy, Shin et al. (9) observed higher elongation and strain hardening in the cryogenic temperature range to be governed by spacing between super dislocations. Smaller spacing at 77 K and wider spacing at 294 K, indicative of a homogeneous slip mode at liquid nitrogen temperature and localized deformation mode at room temperature, has been observed.

The dislocation mechanism observations indicate that although delaminations occur at cryogenic temperatures in Al-Li alloys, homogeneous deformation mode in the laminates created between the delaminations have a higher ductility that give rise to an overall higher toughness. This argument appears to be reasonable irrespective of whether strain hardening exponent increases at cryogenic temperatures or not.

The present study was undertaken to examine if delaminations would occur in sheet material and, if they indeed occurred, what

role would they play in controlling toughness at cryogenic temperatures. To achieve this objective, two 2091 sheets with different thicknesses were chosen for the study.

SECTION 3 EXPERIMENTAL PROCEDURES

The test material investigated in this effort was Al 2091-T3 sheet produced by ALCOA. Two sheet thicknesses were examined: 1.6 and 3.6 mm (0.063 and 0.144 inch, respectively). Tensile specimens were taken from the full thickness of each sheet, with gage section dimensions approximately 6.4 mm (0.25 inch) in width with a 25.4 mm (1.00 inch) gage length. Specimens were removed from various orientations of each sheet to examine for any anisotropy in strength properties, with the loading directions (relative to the rolling direction) of 0, 45, 60, and 90 degrees.

For toughness determination, C(T) specimens were removed from the 3.6 mm (0.144 inch) sheet, with the width (W) of 38 mm (1.5 inches) and thickness equal to the full sheet thickness. Because of anticipated buckling problems with the thinner gage material, M(T) specimens were removed from the 1.6 mm (0.063 inch) sheet, with W equal to approximately 102 mm (4.0 inches). Again, toughness properties for both product thicknesses were examined for the various sheet directions: 0 (L-T), 30, 45, 60, and 90 (T-L) degrees.

Tensile testing was performed in a 10-KIP capacity Instron Universal testing machine at 294, 77, and 4 K (70, -321, and -450°F, respectively), following guidelines set forth in ASTM E-8 Tensile Testing of Metallic Materials. For the 77 K tests the samples were totally immersed in liquid nitrogen, with strain monitored with a cryogenic extensometer. Testing at 4 K was performed in a liquid helium dewar modified with a special testing insert to perform tensile type loading. Again the sample was continually submerged in liquid helium for the duration of the test, with specimen strain obtained via strain gages affixed to the gage section.

Toughness testing was performed using those procedures outlined in ASTM Practice E-561 for R-Curve Determination. A data acquisition system, developed for an HP Model 216 computer system, was used to obtain continuous records of K_r versus effective crack

extension. Compliance methods were used to monitor effective crack length at the test temperatures previously described.

SECTION 4 RESULTS AND DISCUSSION

Actual chemical composition of both sheets used in the present investigation are shown in Table 1. Optical micrographs of the grain structure in the three planes of the two sheets are shown in Figure 1. The grain size in the 1.6 mm sheet is substantially smaller, and the grain shape in the rolling plane is more equiaxed resulting in a reduced length of the continuous high angle grain boundaries as compared to the 3.6 mm sheet. However, extremely long grain boundaries (of the order of millimeters) in directions normal to the thicknesses are observed for both sheets.

Tensile properties at 294, 77, and 4 K are shown in Table 2 for both 1.6 and 3.6 mm sheets as a function of sheet orientation. The variation in strength and ductility as a function of specimen orientation is shown in Figure 2, for the 3.6 mm sheet. Both at room temperature and liquid nitrogen, a minimum in the yield strength and a maximum in the % elongation is observed around 45 degrees. These observations along with the significant increase in yield and ultimate tensile strength at cryogenic temperatures (in all orientations), is similar to the behavior of other Al-Li alloys. The lowest strength and the highest tensile elongation in the neighborhood of 45 degrees can be explained by the texture produced during the processing (in this case rolling) of the material. As shown in Figure 1, although the grains in the rolling plane appear to be equiaxed, substantial alignment of the grains exists in the other two planes, suggesting that a strong texture still prevails in both sheet materials which results in in-plane anisotropy of mechanical properties. Since ductility enhancement of Al-Li alloys at cryogenic temperatures has been rationalized in terms of strain hardening rate and exponent, strain hardening exponents were calculated for the present alloys and are included in Table 2. The difference in strain hardening exponents (n) between 294 and 77 K is so small that not much significance can be attached to this change. Unlike earlier observations on 2090 and 8090 (1-6,8,9,10), ductility of the

TABLE 1

NOMINAL CHEMICAL COMPOSITION OF 2091 SHEETS IN WEIGHT PERCENT

Product	Li	Cu	Mg	Fe	Si	Mn
1.6 mm	1.68	2.17	1.57	0.1	0.1	0.09
3.6 mm	1.71	1.99	1.24	0.1	0.1	0.09

Cr, Zr, Ti and Zn not detected.

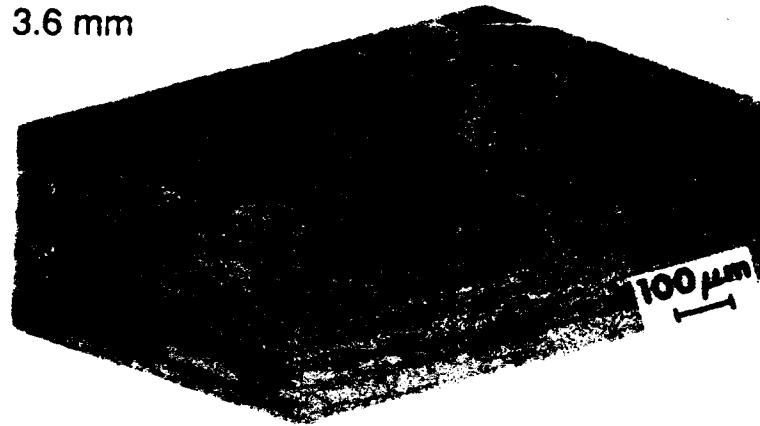
Cr 0.06% if present.

Zr 0.1% if present.

Ti 0.05% if present.

Zn 1.0% if present.

3.6 mm



(a)

1.6 mm



(b)

Figure 1. Optical Microstructure Showing the Grain Structure in the 3.6 mm (a) and 1.6 mm (b), Thick 2091 Sheet Alloy.

TABLE 2
TENSILE PROPERTIES OF THE 3.6mm AND 1.6mm 2091 SHEETS AT 294K, 77K AND 4K

Sheet Thickness mm (inch)	Orientation (Relative to Roll Direction)	Test Temperature K (°F)	Yield Strength MPa (KSI)	Ult. Tensile Strength MPa (KSI)	% Elong. (in 25 mm G.L.)	Strain Hardness Exponent (n)
3.6 (0.144)	0	294 (70)	348 (50.5)	420 (60.9)	19	0.08
3.6 (0.144)	45	294 (70)	282 (40.9)	414 (60.1)	20	0.12
3.6 (0.144)	60	294 (70)	297 (43.1)	423 (61.3)	19	0.11
3.6 (0.144)	90	294 (70)	325 (47.2)	439 (63.7)	14	0.12
3.6 (0.144)	0	77 (-321)	409 (59.3)	547 (79.3)	16	0.09
3.6 (0.144)	45	77 (-321)	328 (47.5)	513 (74.4)	13	0.15
3.6 (0.144)	60	77 (-321)	352 (51.0)	542 (78.6)	18	0.12
3.6 (0.144)	90	77 (-321)	372 (54.0)	574 (83.2)	11	0.15
3.6 (0.144)	0	4 (-450)	477 (69.2)	616 (89.4)	11*	--
3.6 (0.144)	90	4 (-450)	445 (64.6)	662 (96.0)	12*	--
1.6 (0.063)	0	294 (70)	328 (47.6)	418 (60.6)	24	0.04
1.6 (0.063)	45	294 (70)	280 (40.6)	419 (60.7)	23	0.12
1.6 (0.063)	60	294 (70)	282 (40.8)	422 (61.1)	22	0.13
1.6 (0.063)	90	294 (70)	295 (42.8)	440 (63.9)	18	0.13
1.6 (0.063)	0	77 (-321)	394 (57.1)	489 (70.9)	14	0.05
1.6 (0.063)	0	4 (-450)	464 (67.3)	530 (76.9)	4.5	--

* 12.7 mm (0.5 inch) gage length.

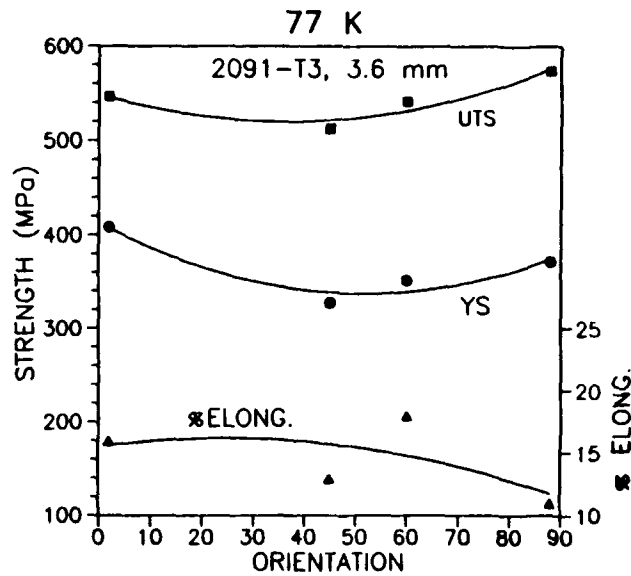
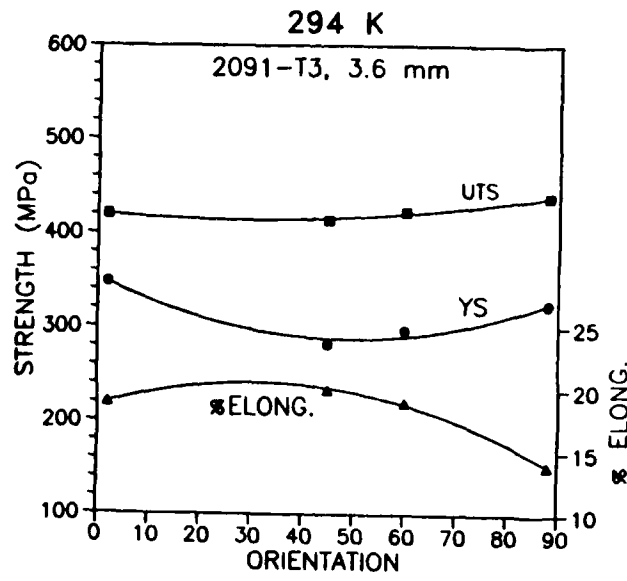


Figure 2. Variation of Yield (YS) and Ultimate Tensile Strengths (UTS) and Percent Elongation as a Function of Specimen Orientation at 294K and 77K.

present 2091 alloys decreases at both 77 and 4 K. These results on strength and ductility obtained in the longitudinal orientation for both sheets and in the transverse orientation for the 3.6 mm sheet are shown as a function of temperature in Figure 3.

To understand the reduction in ductility in terms of dislocation arrangements, slip mode at the two temperatures was studied using thin foils cut from tensile specimens that were strained to 2 percent. Figures 4(a) and (b) show the images obtained under 2-beam conditions. Planar dislocation arrays at 77 K and tangled dislocation networks at 294 K are observed. These observations appear to be consistent with the brittle nature of the alloy at 77 K and are thus postulated to be a reason for the reduction in ductility along the model proposed by Ashby et al. (11), who recently showed that brittle behavior could be exhibited by a material if dislocation generation is suppressed.

The differences in the dislocation arrangements result in a substantial difference in the fracture characteristics at ambient and cryogenic temperatures. As will be noted later, these features are accentuated in the presence of a notch. The comparison between the failure modes at ambient and cryogenic temperatures is shown in Figure 5, for the longitudinal orientation. Low magnification pictures (Figures 5(a-c)) show that complete delaminations (i.e. deeper and longer) occur only at liquid nitrogen temperature and below. At 294 K delaminations are incomplete, in the sense that they are neither deeper nor do they cover a major portion of the width of the specimen. As shown in the high magnification micrographs (Figures 5(d-f)), fracture occurs by a mixture of transgranular slip band (or shear) cracks and intergranular failure at 77 K and below, whereas at 294 K fracture occurs by ductile transgranular microvoid coalescence. The term 'brittle fracture mode' has been used here for transgranular slip band cracking and intergranular cracking. Fractographic features on tensile specimens tested in other orientations of the 3.6 mm sheet and 1.6 mm sheet are approximately similar and do not warrant discussion.

R-curves for the 3.6 mm sheet loaded in various orientations at ambient and liquid nitrogen temperatures are shown in Figure 6,

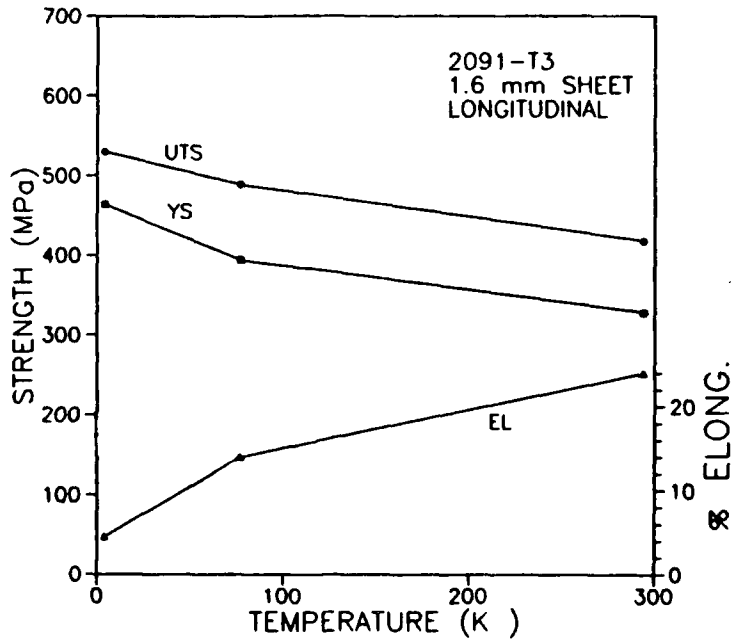
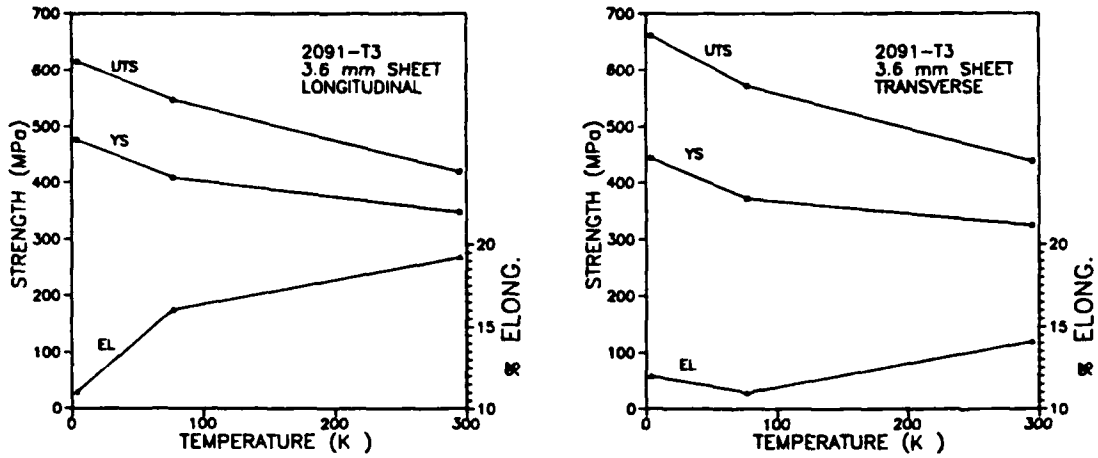


Figure 3. Effect of Temperature on the Tensile Properties in the Longitudinal and Long-Transverse Orientation for the 3.6mm and Longitudinal Orientation for the 1.6mm.



Figure 4. TEM Micrographs Showing the Dislocation Structures at 294K and 77K.

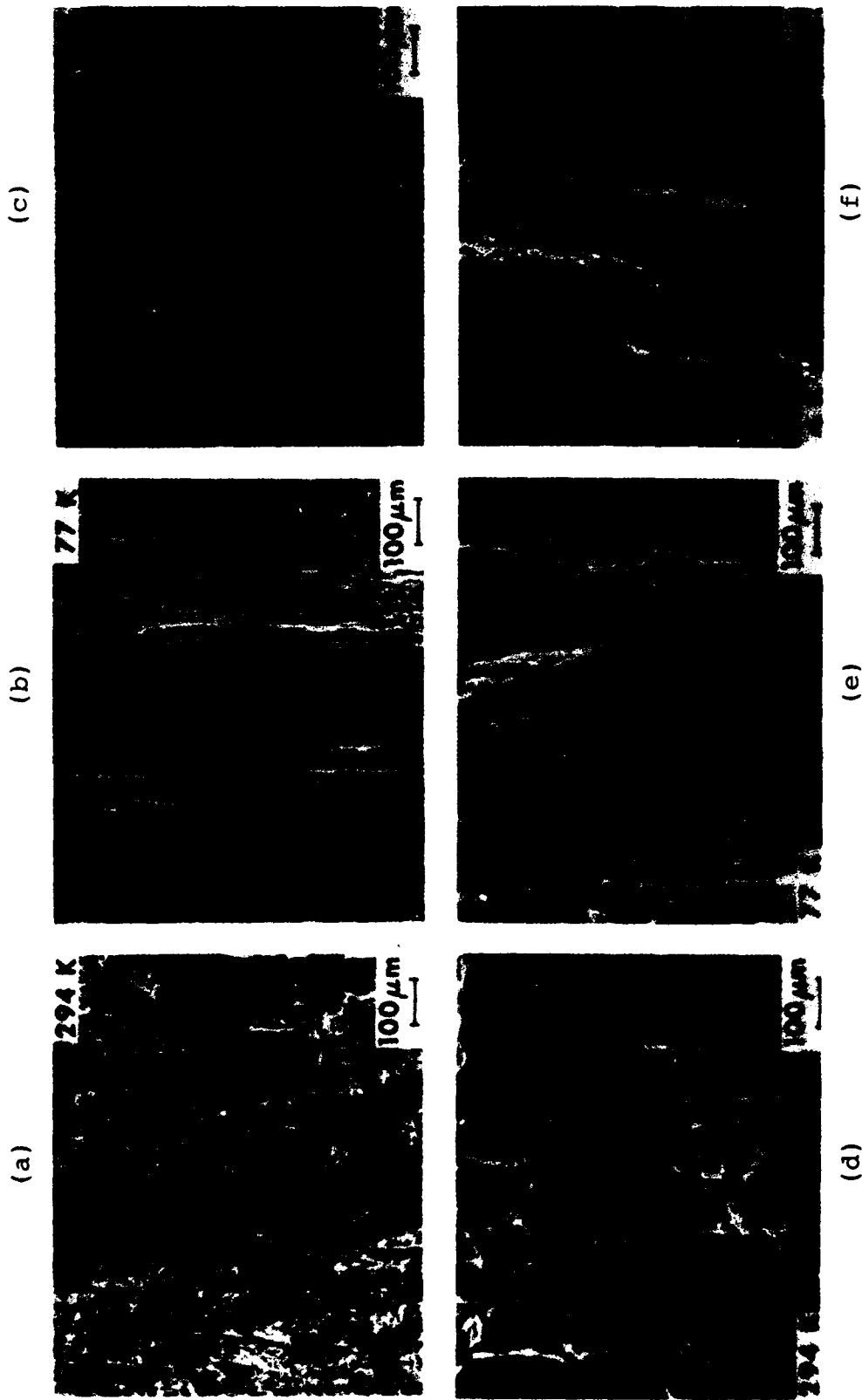


Figure 5. Low Magnification Fractographs in Longitudinal Tensile Samples at (a) Room Temperature, (b) Liquid Nitrogen, (c) Liquid Helium Temperatures. Note Delaminations in (b) and (c). Figure 5(d) Shows the Ductile Failure at Room Temperature and 5(e) and 5(f) Show the Brittle Failure at Cryogenic Temperatures.

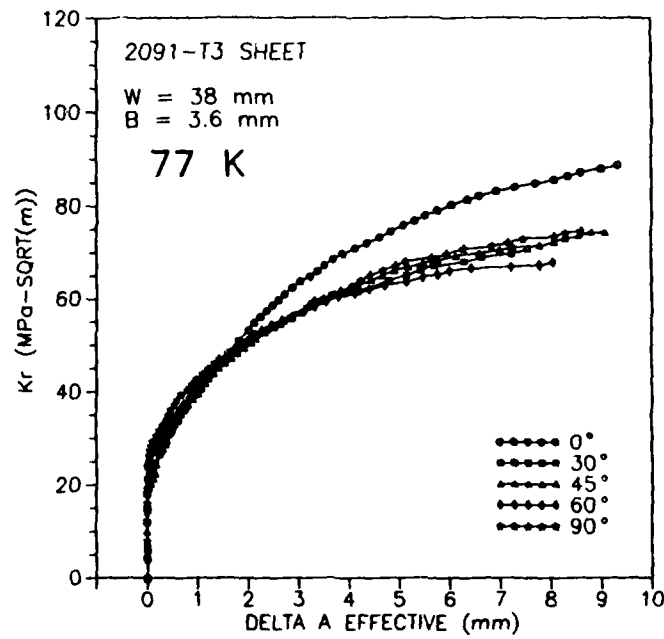
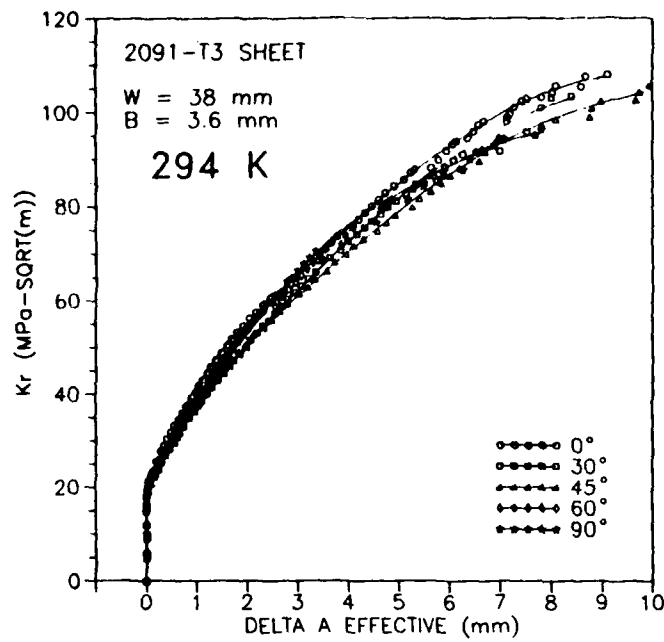
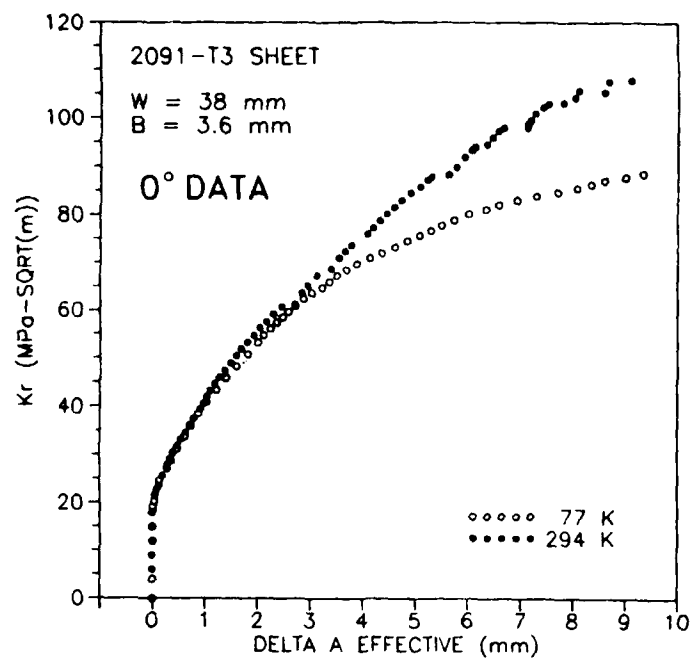


Figure 6. Effect of Orientation on the R-Curves at 294K and 77K for the 3.6mm Sheet.

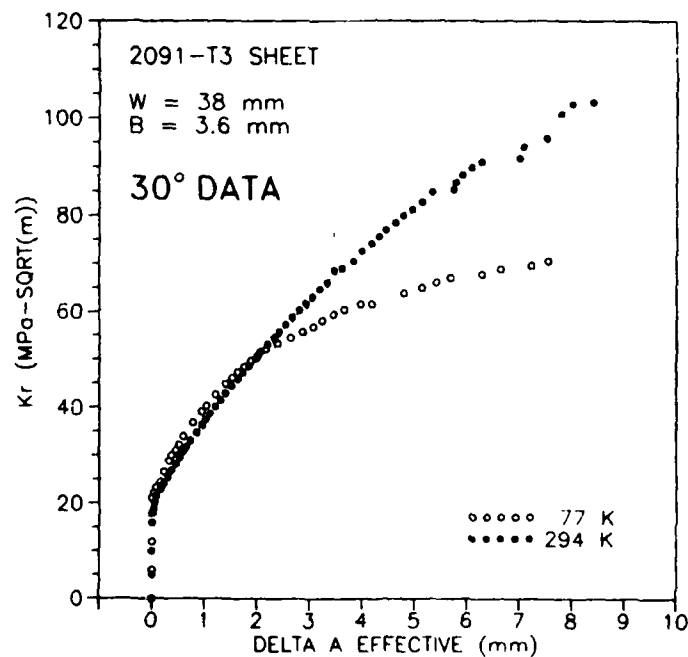
while the effect of temperature for each orientation is shown separately in Figures 7(a-e). At both temperatures and for crack extensions longer than 2 mm, R-curve for the 0 degree orientation lies above the curves of other orientations, indicating a higher crack growth resistance. This same trend is also seen for the 1.6 mm thick material, shown in Figures 8 and 9.

For all orientations, the resistance curves of the 3.6 mm material at liquid nitrogen conditions fell consistently below the ambient test results. For the 1.6 mm M(T) samples, such a drop is not as apparent, though the resistance curves at liquid nitrogen temperatures were terminated (due to specimen fracture) over a small range of effective crack extension as shown in Figures 9(a-d).

As discussed above, both the 3.6 mm and 1.6 mm sheet materials exhibited qualitatively similar toughness, i.e. rising R-curves. Values of $K_{r-25\%}$, a value of K on the R-curve based on a 25% secant intercept of the load-displacement curve which can be used as per ASTM B646 as toughness correlator for the C(T) specimen, are shown in Table 3 for the 3.6 mm sheet. Also shown are the values of K_{r-max} , a value of K on the R-curve based on maximum load and corresponding effective crack length. K_{r-max} values for the 1.6 mm sheet are shown in Table 4. $K_{r-25\%}$ values for the center cracked panels have been intentionally omitted from Table 4 since the testing standard suggests only K_{r-max} values for this geometry. Quantitative comparisons between the two sheets, as shown in Tables 3 and 4, need to be cautiously made since 3.6 mm material was tested in the form of compact tensions, whereas the 1.6 mm material was tested as center cracked panels. However, some testing was performed on center cracked panels of 3.6 mm material reduced to a thickness of 1.6 mm, to find if any difference in R-curve behavior between the two sheet thicknesses exists for an identical specimen geometry. The results, as shown in Figure 10, indicate similar R-curve behavior for the two sheets but a slightly lower toughness (K_{r-max}) for the reduced 3.6 mm sheet. Thus, the smaller values of K_{r-max} for the 3.6 mm sheet as

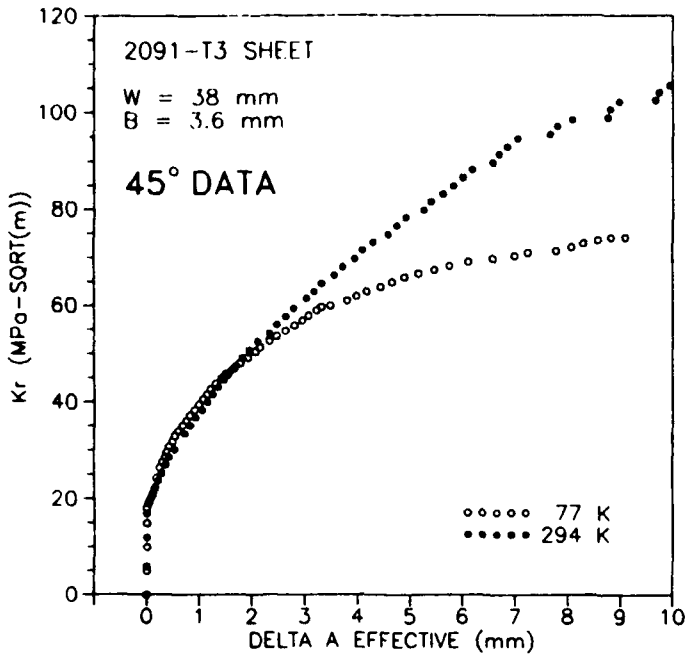


(a)

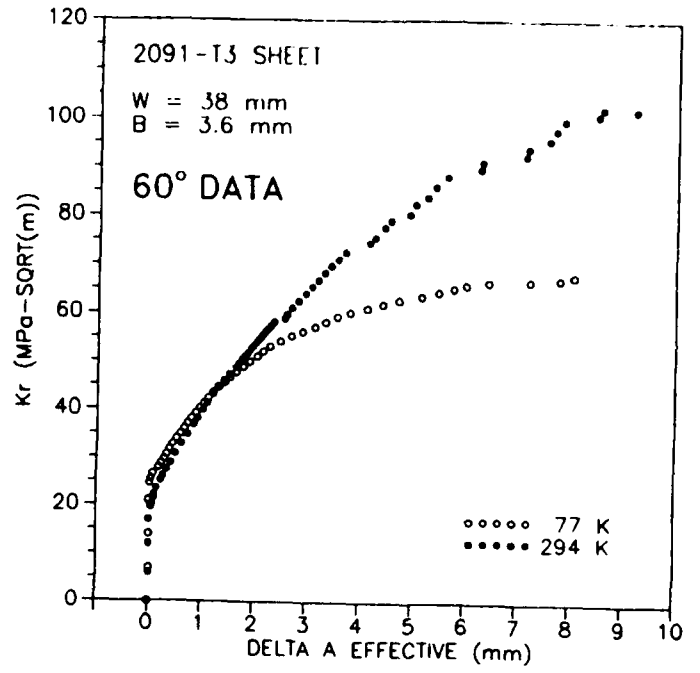


(b)

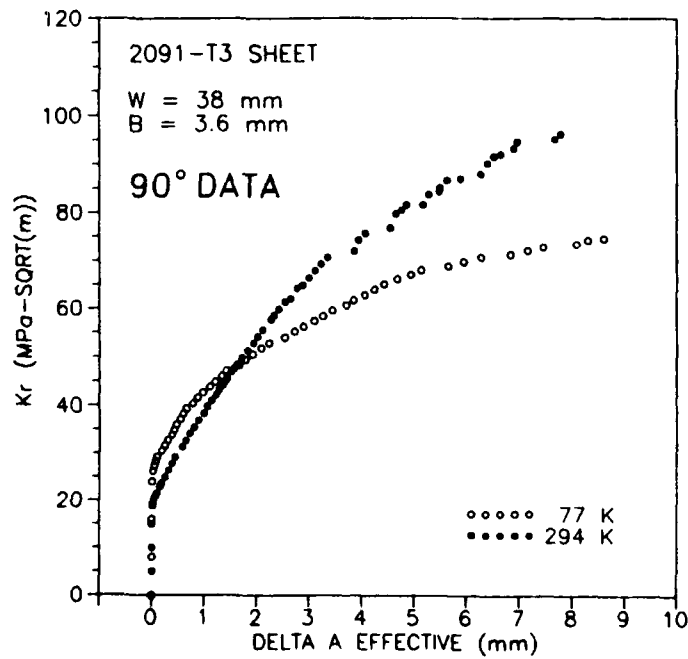
Figure 7. Effect of Temperature (294 vs. 77K) on the R-Curves for (a) 0°, (b) 30°, (c) 45°, (d) 60° and (e) 90° Orientations, for the 3.6mm Sheet.



(c)



(d)



(e)

Figure 7 (Concluded)

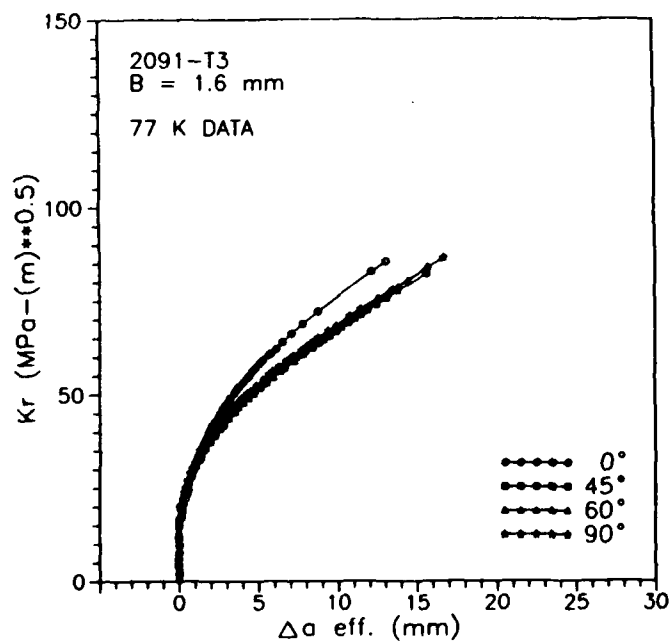
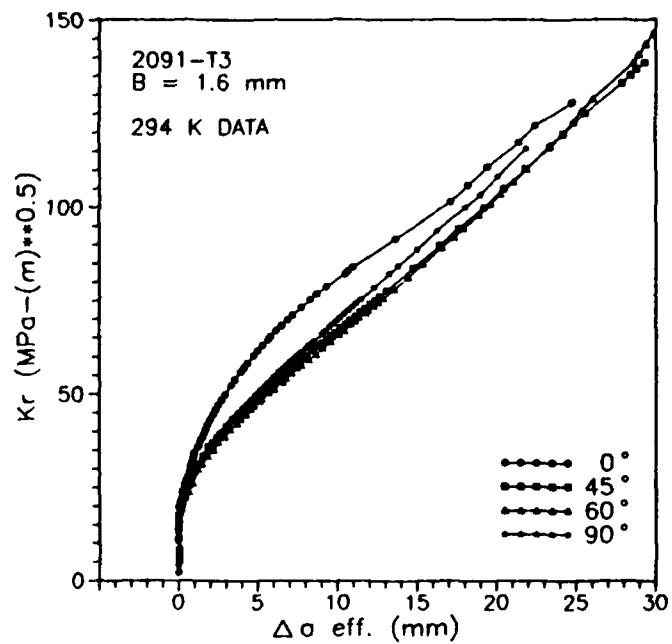


Figure 8. Effect of Orientation on the R-Curves at 294 and 77K for the 1.6mm Sheet.

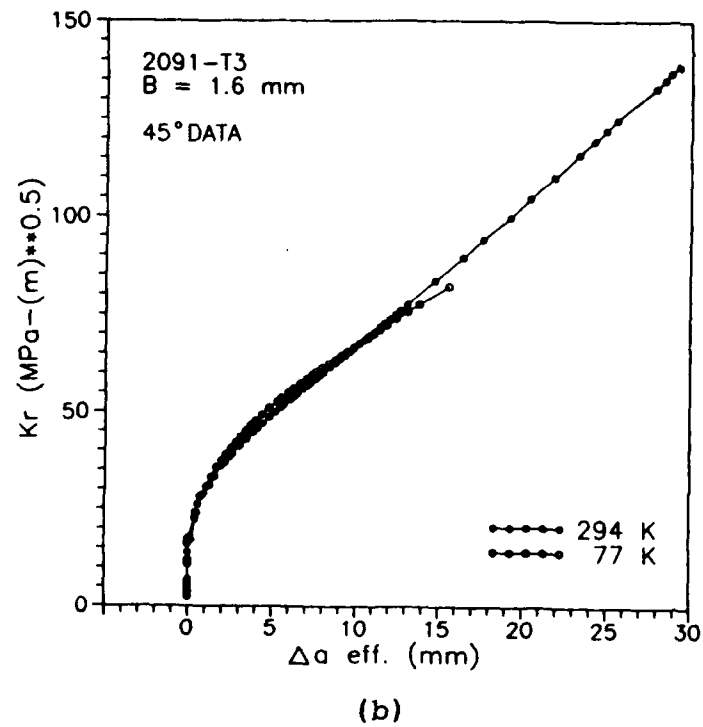
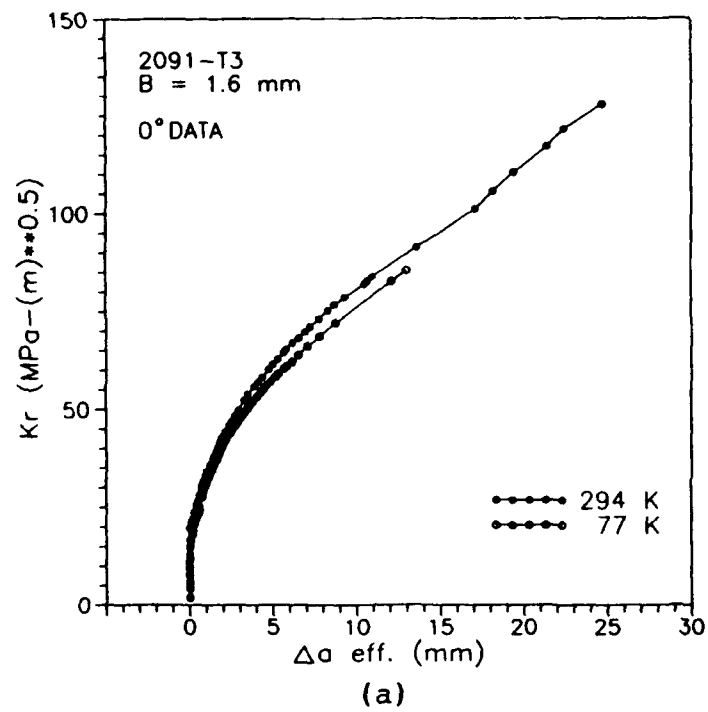


Figure 9. Effect of Temperature (294 vs. 77K) on the R-Curves (a) 0°, (b) 45°, (c) 60°, and (d) 90° Orientations for the 1.6mm Sheet.

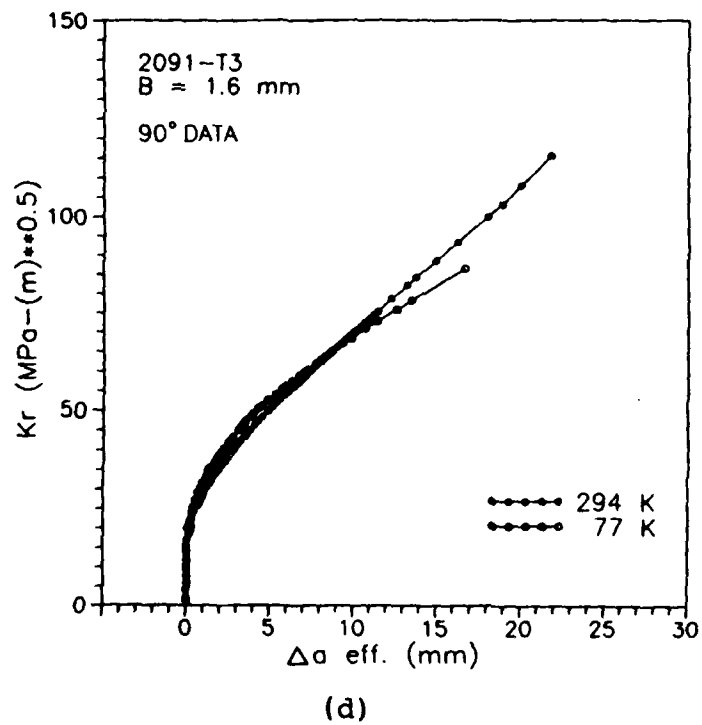
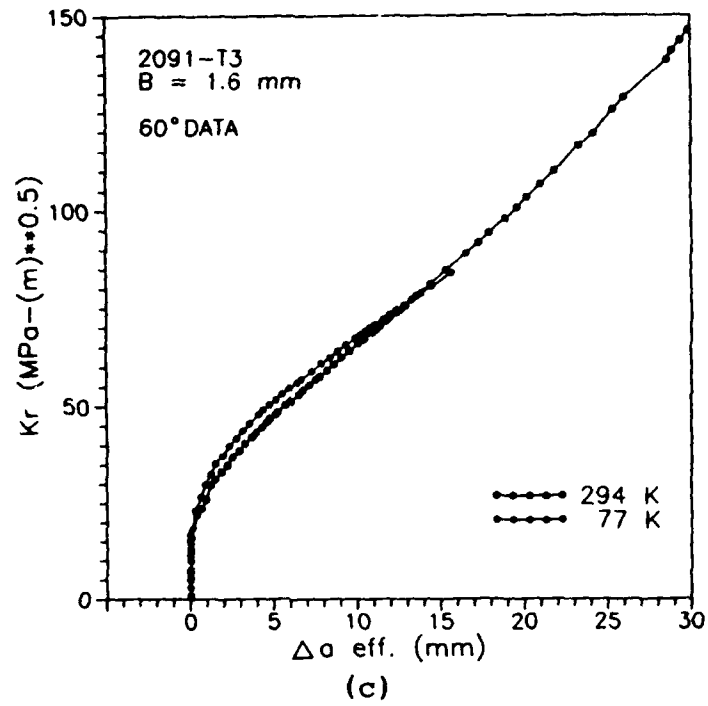


Figure 9 (Concluded)

TABLE 3

Kr-25% AND Kr-max VALUES AT 294K AND 77K AT VARIOUS ORIENTATIONS
FOR THE 3.6mm THICK 2091-T3 ALLOY, C(T) SPECIMENS

Orientation (Deg)	Temperature		Kr _{25%}		Kr _{max}	
	K	(F)	MPa√m	(KSI√in)	MPa√m	(KSI√in)
0	294	(70)	60	(55)	88	(80)
30	"	"	58	(53)	92	(84)
45	"	"	56	(51)	89	(81)
60	"	"	64	(58)	93	(85)
90	"	"	57	(52)	81	(74)
0	77	(-321)	57	(52)	69	(63)
30	"	"	54	(49)	60	(55)
45	"	"	52	(47)	59	(54)
60	"	"	51	(46)	56	(51)
90	"	"	53	(48)	65	(59)

TABLE 4

Kr-max VALUES AT 294K AND 77K AT VARIOUS ORIENTATIONS FOR
THE 1.6mm THICK 2091-T3 ALLOY, M(T) SPECIMENS

Orientation (Deg)	Temperature		Kr _{25%}		Kr _{max}	
	K	(F)	MPa√m	(KSI√in)	MPa√m	(KSI√in)
0	294	(70)	65	(59)	96	(87)
45	"	"	53	(48)	125*	(114)*
60	"	"	48	(44)	149*	(136)*
90	"	"	52	(47)	115*	(105)*
0	77	(-321)	59	(54)	86	(78)
45	"	"	54	(49)	77	(70)
60	"	"	55	(50)	84	(76)
90	"	"	54	(49)	73	(66)

*Invalid due to net section yielding.

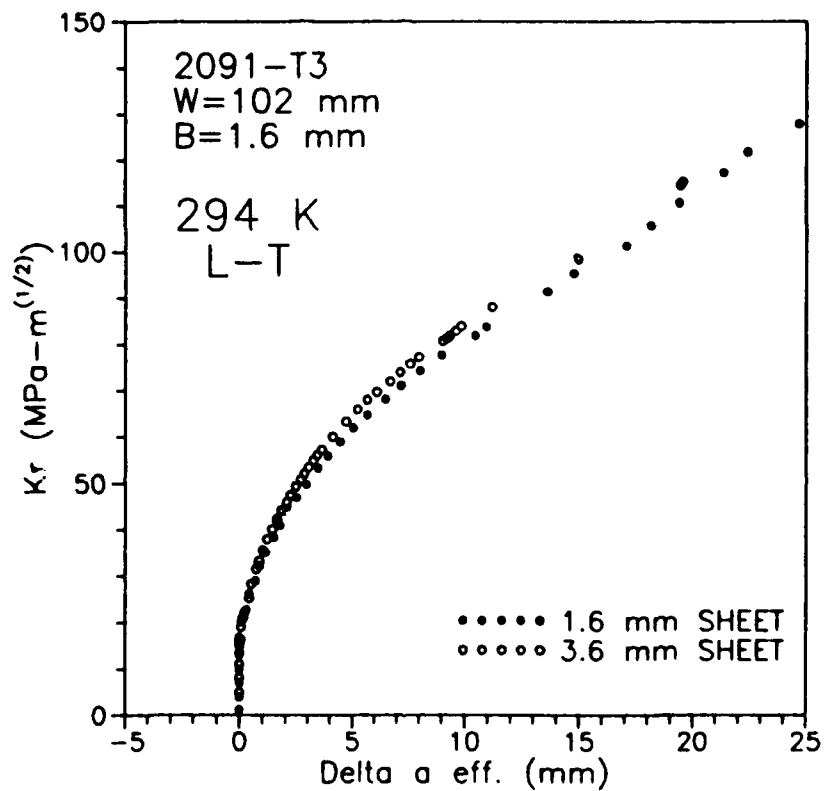


Figure 10. (a) Comparison of R-Curve Behavior of the 3.6mm Sheet Reduced to 1.6mm and Tested in Center Cracked Specimen Configuration to the Compact Tension Specimen

compared to the 1.6 mm material for the present 2091 sheets appears to be related to microstructural differences, i.e. grain size, between the two sheets.

At liquid nitrogen temperature, both sheets could not sustain large crack extensions and thus Kr curves at liquid nitrogen temperature appeared curtailed at lower values of crack length increment. This behavior is pronounced in the thinner sheet as exemplified in Figure 11, where load-displacement curves for approximately similar starting fatigue precracks are compared for 294 and 77 K. The early curtailment of crack growth resistance at 77 K appears to be related to the brittle failure mode as shown in the associated micrograph in Figure 11.

At ambient temperature, specimens oriented in the longitudinal direction (0 degrees) failed by a microvoid coalescence mechanism. As the orientation of the stress axis changed towards 90 degrees with respect to the rolling direction microvoid coalescence progressively decreased and delaminations along grain boundaries increased. In the T-L orientation (90 degrees to the rolling direction) failure by microvoid coalescence is sparse and the predominant mode of failure is slip band and grain boundary cracking with intense delaminations along the through-the-thickness of the specimen. Micrographs showing these fractographic results are shown in Figures 12-16.

At liquid nitrogen temperature all specimens exhibited delaminations and brittle failure. These results suggest that a delamination toughening mechanism does not produce any improvement in fracture toughness at 77 K in this material. The fracture toughness trend shown in terms of Kr-25% and Kr-max in Figure 17 consistently shows that the values are lower at 77 K. The fracture mode transition from ductile microvoid coalescence to slip band plus grain boundary fracture is the factor that is decreasing the fracture toughness at cryogenic temperatures in the present materials.

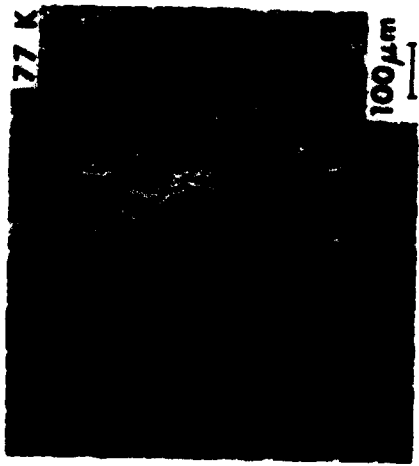
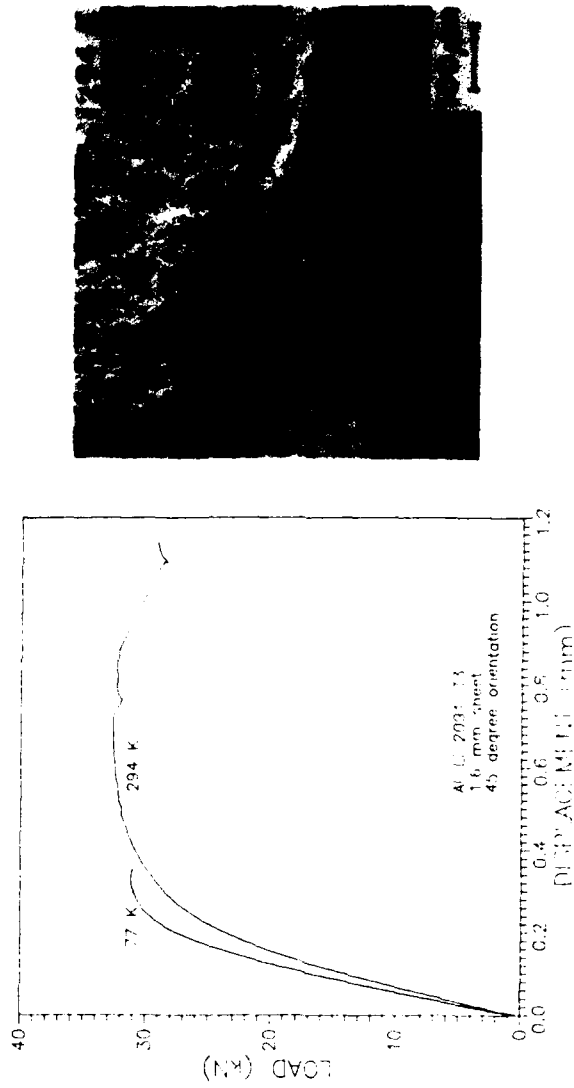
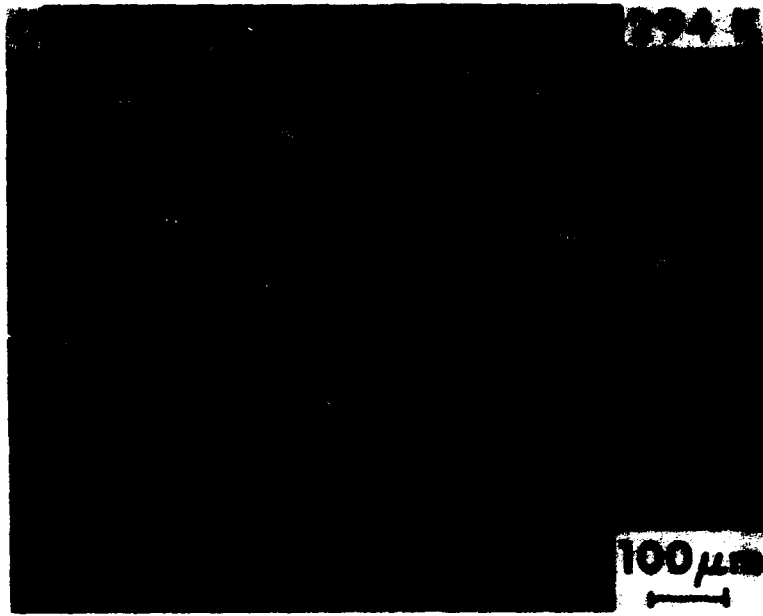
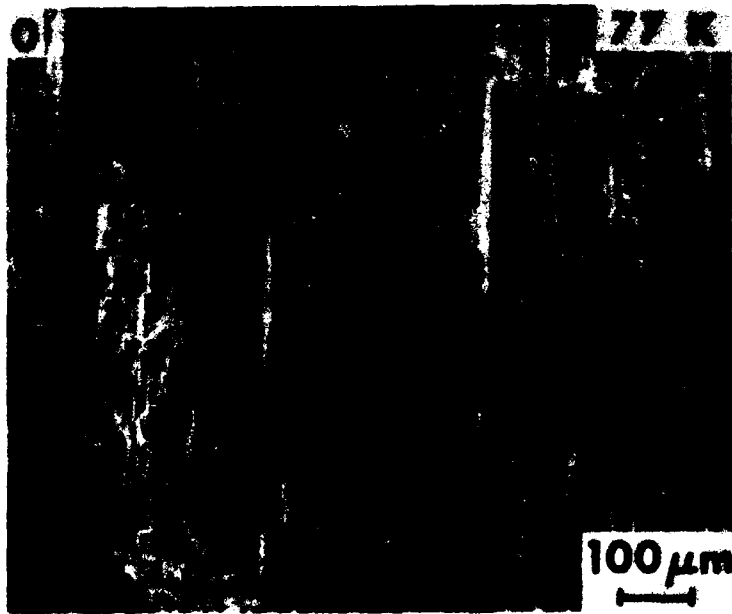


Figure 11. Load Versus Crack Opening Displacement Curves for Two Center Cracked Panels (45° Orientation) with Similar Fatigue Precrack Lengths Showing the Inability to Sustain Stable Crack Extension at Liquid Nitrogen Temperature. Notice in the Fractographs the Ductile Failure Mode at 294K and Brittle Failure Mode at 77K.

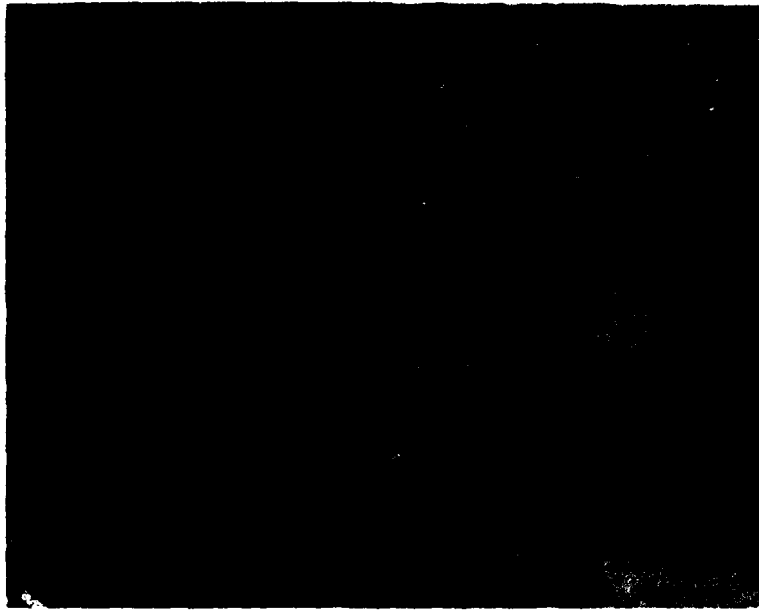


(a)

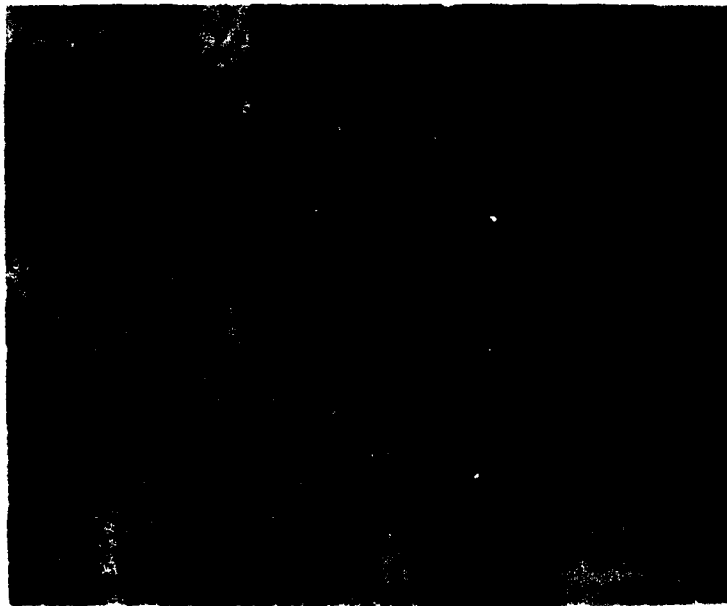


(b)

Figure 12. SEM Fractographs Showing (a) Failure by Ductile Microvoid Coalescence at 294K and (b) Brittle Intergranular and Slip Band Cracking at 77K, for the 0° Oriented R-Curve Specimen.

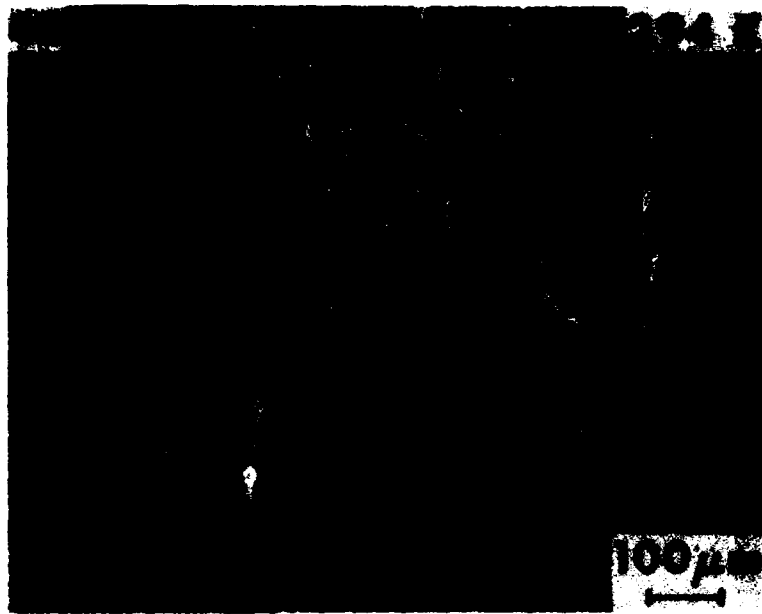


(a)

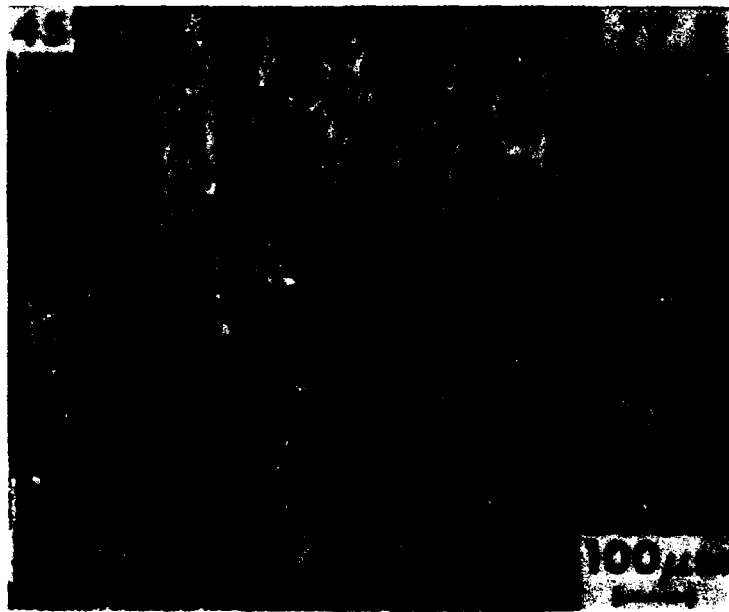


(b)

Figure 13. SEM Fractographs Showing (a) the Ductile Microvoid Coalescence with Delaminations Associated with Grain Boundaries at 294K and (b) Larger Number of Delaminations with Brittle Intergranular and Slip Band Cracking at 77K. R-Curve Specimen Oriented 30 Degrees to the Rolling Direction.



(a)



(b)

Figure 14. Mechanism of Failure in the 45° Oriented R-Curve Specimen at 294K (a) and 77K (b) is Similar to that of the 30° Oriented Specimen.

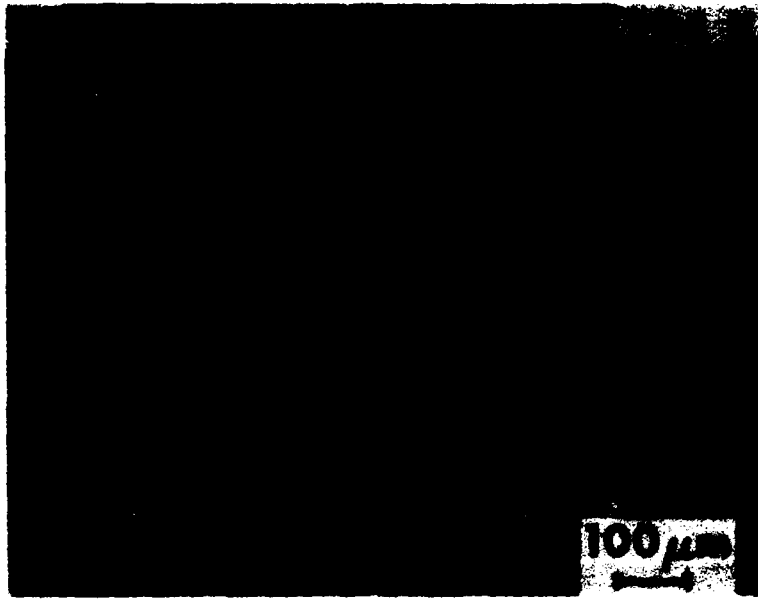


(a)

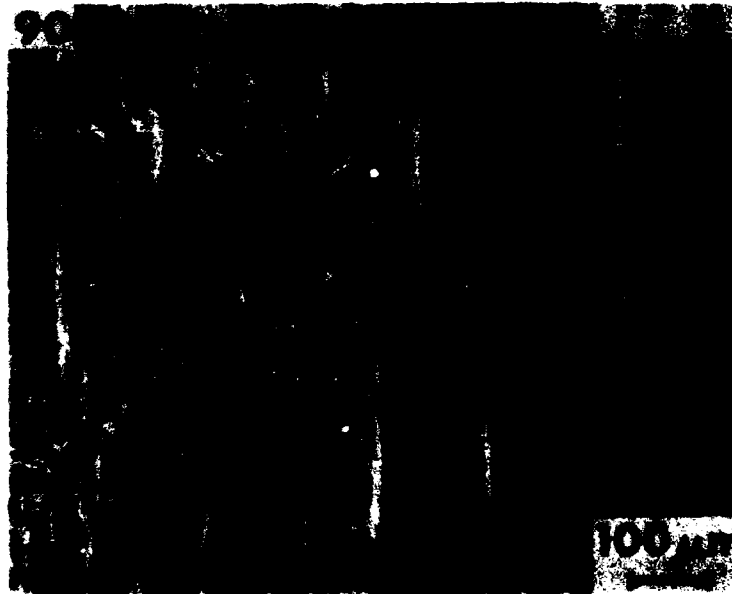


(b)

Figure 15. SEM Fractographs Showing (a) Larger Number of Delaminations Occurring at 294K in the 60° Oriented R-Curve Specimen as Compared (b) Brittle Failure and Delaminations at 77K.



(a)



(b)

Figure 16. SEM Fractographs Showing that the Failure at (a) 294K in 90° Oriented R-Curve Specimen is Largely by Delaminations and Some Microvoid Coalescence; and at 77K Brittle Failure with Delaminations, (b).

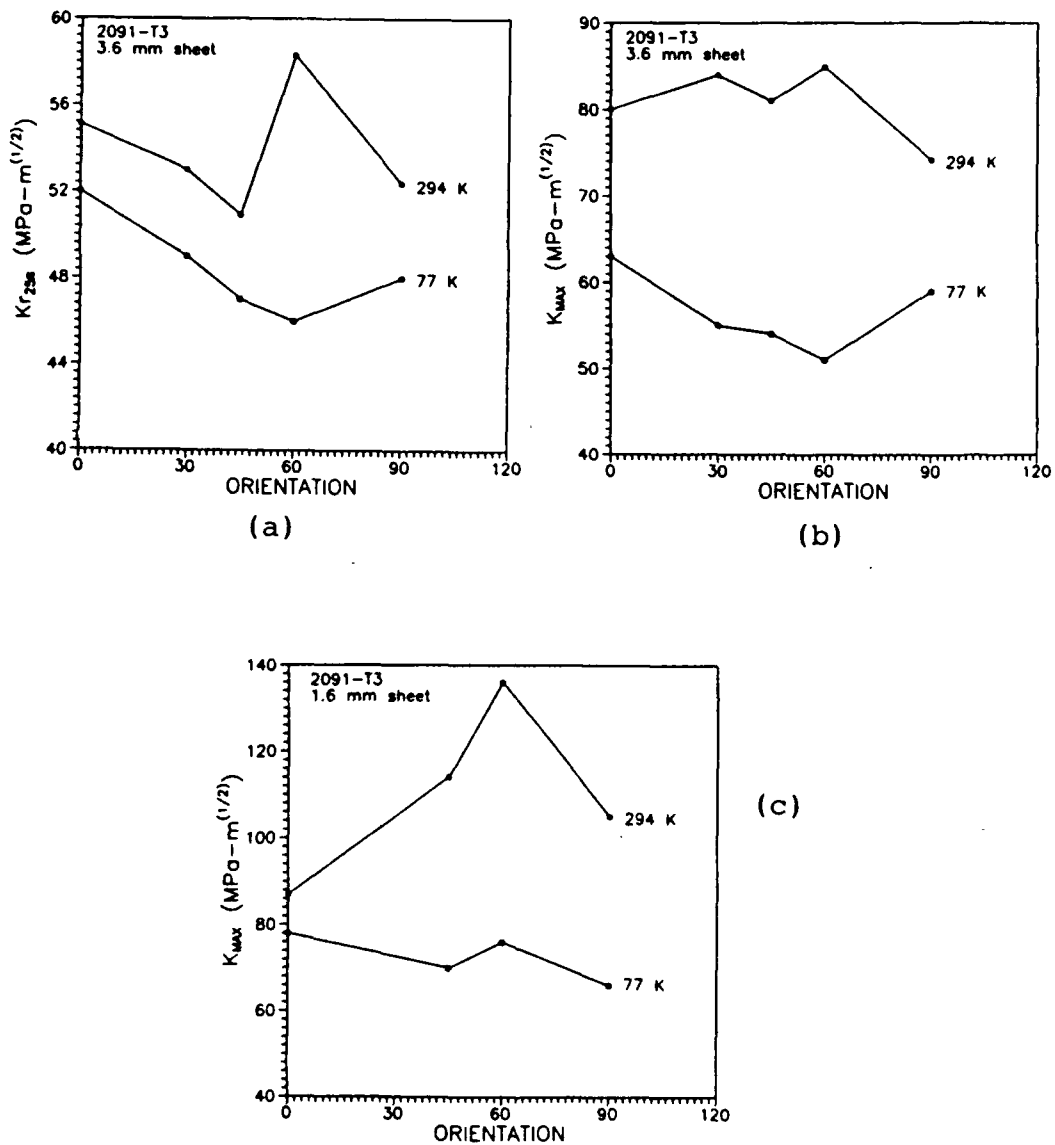
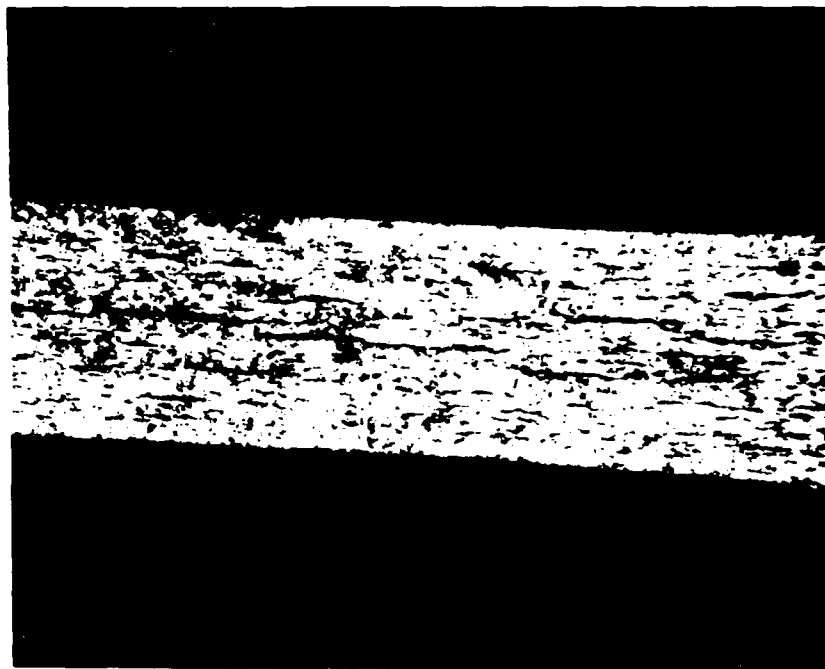


Figure 17. Values of Kr-25% and Kr-maximum at 294K and 77K as a Function of Orientation of the 3.6 mm R-Curve Specimens, (a) and (b); and Kr-maximum Values for the 1.6 mm Sheet (c).

SECTION 5
REMARKS ON PRESENT FINDINGS

Since it is well known that Al-Li alloys have inherently weak short-transverse properties and the high angle grain boundaries can fracture at cryogenic temperatures, the present study was undertaken on sheet material hoping to avoid these factors. From the present study it is clear that the behavior of Al-Li alloys could still be very puzzling. The most unexpected result is the through-thickness delaminations at cryogenic temperatures, in sheets as thin as 3.6 and 1.6 mm, as shown in Figure 18. This result is surprising, since we would expect the triaxial constraint and hence the through-thickness stress in thin sheet to be minimal. Microstructurally, the T3 temper that was chosen for the present study did not contain any harmful equilibrium grain boundary precipitates or precipitate free zones. However, grain shape in the L-S and T-S planes, as was pointed out and shown in Figure 1, is highly elongated and the grain boundaries run several millimeters long. The present study has revealed some important results on the mechanical behavior and associated fracture mechanisms of 2091 sheet material at cryogenic temperatures. However, understanding of the fracture modes is still incomplete. More work needs to be performed, and a number of newer alloys such as Weldalite® and latest versions of 2090, 2091 and 8090 alloys need to be investigated for their cryogenic performance in as-received and as-welded conditions. At cryogenic temperatures, interior of the grains may harden to a much higher stress than the grain boundaries. It is envisaged that stresses that may build up at the grain boundaries due to the elevated strength of the grain interior may crack the grain boundaries by a stress controlled fracture mechanism.



(a)



(b)

Figure 18. Macrophotographs Showing Delaminations in Both (a) 1.6mm and (b) 3.6mm Sheets.

SECTION 6
CONCLUSIONS

The present investigations on 2091 sheet materials lead to the following conclusions.

1. Strength and ductility can be related to rolling texture that is prevalent in these materials. A minimum in strength and a corresponding maximum in ductility occurs around 45 degrees.
2. Yield and ultimate strength increase at cryogenic temperatures in all orientations by 15 to 30 percent.
3. Ductility is decreased at cryogenic temperatures in all orientations.
4. Crack growth resistance as measured by R-curves is decreased at cryogenic temperatures in all orientations.
5. The decrease in tensile ductility and crack growth resistance is related to an inability to produce mobile dislocations ahead of the crack tip.
6. The decrease in toughness can be related to a change in the fracture mode. At ambient temperature, fracture occurs by ductile microvoid coalescence, whereas at cryogenic temperatures, fracture occurs by slip band and intergranular cracking.

REFERENCES

1. D. Webster, "Aluminum-Lithium Alloys III," The Institute of Metals, London, 1986, pp. 602-609.
2. R.C. Dorward, *Scripta Metallurgica*, 1986, Vol. 20, pp. 1379-83.
3. J. Glazer, S.L. Verzasconi, R.R. Sawtell, and J.W. Morris, *Metall. Trans.*, 1987, Vol. 18A, pp. 1695-1701.
4. K.T. Venkateswara Rao, W. Yu, and R.O. Ritchie, *Metallurgical Transactions*, Vol. 20A, 1989, pp. 485-497.
5. J. Glazer, S.L. Verzasconi, E.N. Dalder, W. Yu, R.A. Emigh, R.O. Ritchie, and J.W. Morris, Jr., *Advances in Cryogenic Engineering*, 1986, pp. 397.
6. K.V. Jata and E.A. Starke, Jr., *Scripta Metallurgica*, 1988, Vol. 22, pp. 1553-1556.
7. K.S. Chan, *Metallurgical Transactions*, 1989, Vol. 20A, pp. 155-164.
8. K. Welpmann, Y.T. Lee, and M. Peters in "Aluminum-Lithium Alloys, Volume III," *Proceedings of the Fifth International Aluminum-Lithium Conference*, Williamsburg, Virginia, March 27-31, 1989, Published by Materials and Component Engineering Publications Limited, Birmingham, U.K., Editors: T.H. Sanders and E.A. Starke, Jr., pp. 1513-1522.
9. K.S. Shin et al., *ibid*, pp. 1543-1552.
10. D. Dew-Hughes, E. Creed, and W.S. Miller, *Materials Science and Technology*, 1988, Vol. 4, pp. 106-112.
11. M.F. Ashby and J.D. Embury, *Scripta Metallurgica*, 1985, Vol. 19, pp. 557-562.